Supplementary Information (SI) for Journal of Materials Chemistry A.

Supporting Information

Hybrid Zirconium Phosphate Phosphonates as Efficient Hosts for Confined Ni-Fe Oxygen Evolution Catalysts

Anna Donnadio,*[a] Iolanda D'Ambrosio,[b] Gabriel Menendez Rodriguez,[b,c] Ferdinando Costantino,[b] Riccardo Vivani,[a] Stefano Giovagnoli,[a] Alceo Macchioni,[b,c] Beatrice Muzzi,[d] Enrique Rodríguez-Castellón,[e] Morena Nocchetti*[a]

[a] Department of Pharmaceutical Sciences, University of Perugia, via del Liceo 1, 06123 Perugia, Italy

[b] Department of Chemistry, Biology and Biotechnologies, University of Perugia, via del Liceo 1, 06123 Perugia, Italy

[c] CIRCC, Interuniversity Consortium for Chemical Reactivity and Catalysis, Via C. Ulpiani, 27 - 70 126 Bari, Italy

[d] Institute of Chemistry of Organometallic Compounds - CNR, via Madonna del Piano, 10 50019 Sesto Fiorentino (FI) Italy.

[e] Department of Inorganic Chemistry, Institute for Interuniversity Research in Bio-Refineries (I3B), Faculty of Sciences, University of Málaga, 29071 Málaga, Spain.

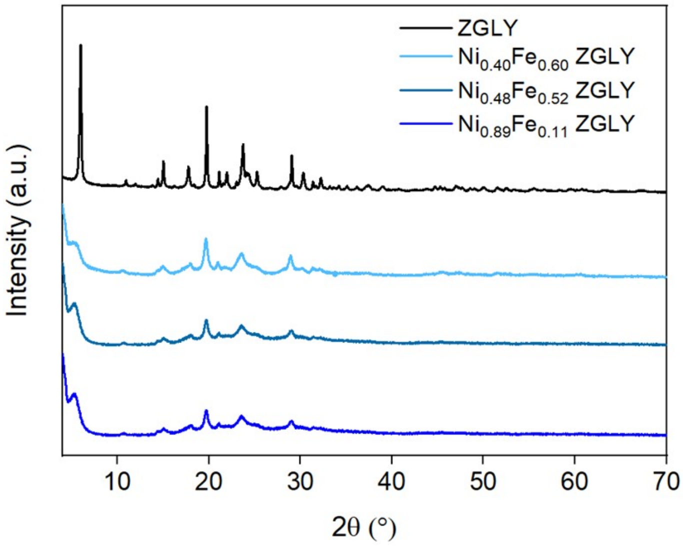

Figure S1. XRD patterns of NiFeZGLY with different Ni/Fe molar ratios. The XRD pattern of ZGLY metal-free was reported for comparison.

Table S1. Surface chemical composition (in atomic concentration %) of NiFeZPACs determined by XPS.

Sample	**C 1*s***	**N 1*s***	**O 1*s***	**P 2*p***	**Fe 2*p***	**Ni 2*p***	**Zr 3*d***
$Ni_{0.68}Fe_{0.32}$ZGLY	30.77	5.98	44.07	11.02	1.82	2.45	3.89
NiFeZGABA	35.14	4.99	41.49	10.55	2.20	1.92	3.80
NiFeZVAL	36.35	4.97	41.69	10.17	1.65	1.43	3.76
NiFeZCAP	38.90	4.70	39.5	9.96	1.77	1.11	3.60

Table S2. Relevant atomic ratios (nominal and found) of NiFeZPACs.

Sample	**$P/Zr_{nominal}$**	**P/Zr_{found}**	**$Zr/N_{nominal}$**	**Zr/N_{found}**	**$C/N_{nominal}$**	**C/N_{found}**
$Ni_{0.68}Fe_{0.32}$ZGLY	2.50	2.86	1.00	0.65	4.00	5.14
NiFeZGABA	2.50	2.78	1.00	0.76	6.00	7.04
NiFeZVAL	2.50	2.70	1.00	0.76	7.00	7.31
NiFeZCAP	2.50	2.78	1.00	0.77	8.00	8.27

Table S3. Binding energy values (in eV) of the constituent elements of NiFeZPACs, and % of the different contributions in brackets.

Sample	**C 1*s***	**N 1*s***	**O 1*s***	**P 2*p***	**Fe 2$p_{3/2}$**	**Ni 2$p_{3/2}$**	**Zr 3$d_{5/2}$**
$Ni_{0.68}Fe_{0.32}$ZGLY	284.7(59) 285.9(30) 288.3(11)	399.7(61) 401.7(39)	531.2(87) 532.8(13)	133.1	710.1	855.4	183.1
NiFeZGABA	284.6(53) 285.7(37) 288.1(10)	399.4(30) 401.7(70)	531.2	133.2	709.5	855.7	183.1
NiFeZVAL	284.7(53) 285.8(38) 288.2(9)	399.5(23) 401.7(77)	531.3(95) 532.9(5)	133.4	709.8	855.5	183.2
NiFeZCAP	284.5(57) 285.8(35) 288.2(8)	399.4(23) 401.6(77)	531.6	133.2	710.0	855.7	183.3

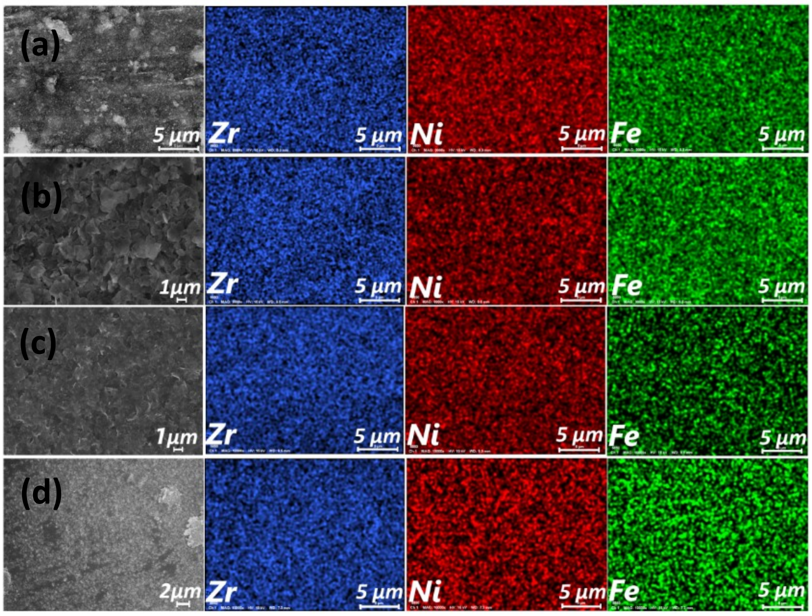

Figure S2. SEM images and EDS element mappings of $Ni_{0.68}Fe_{0.32}$ZGLY (a), NiFeZGABA (b), NiFeZVAL (c), and NiFeZCAP (d).

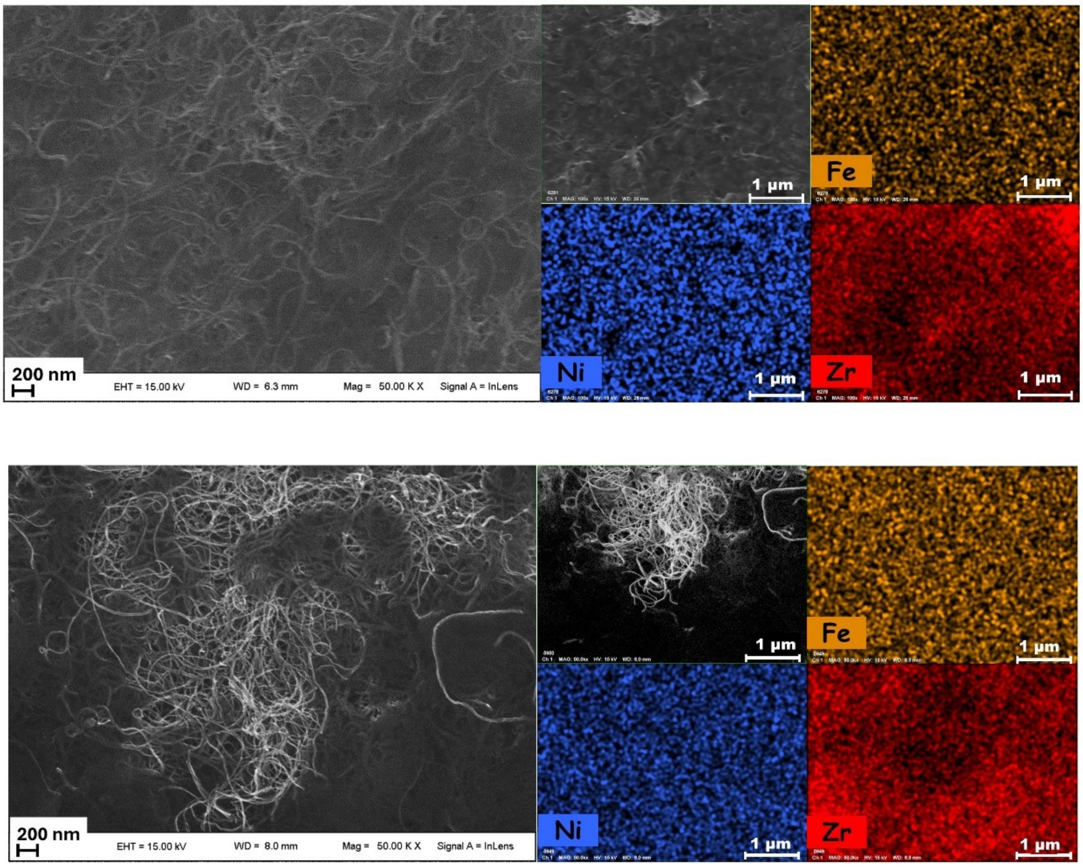

Figure S3. SEM and EDS images of the ink-based $Ni_{0.68}Fe_{0.32}$ZGLY, recorded before (on the top) and after (bottom) electrochemical reaction.

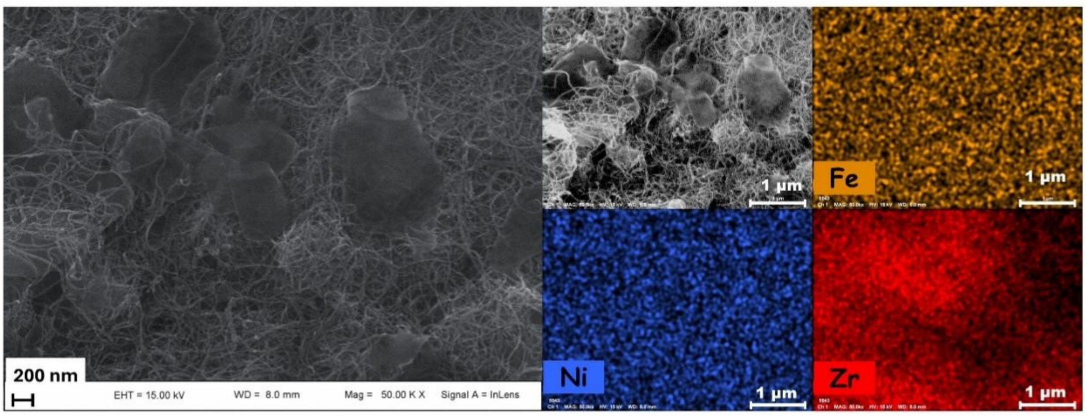

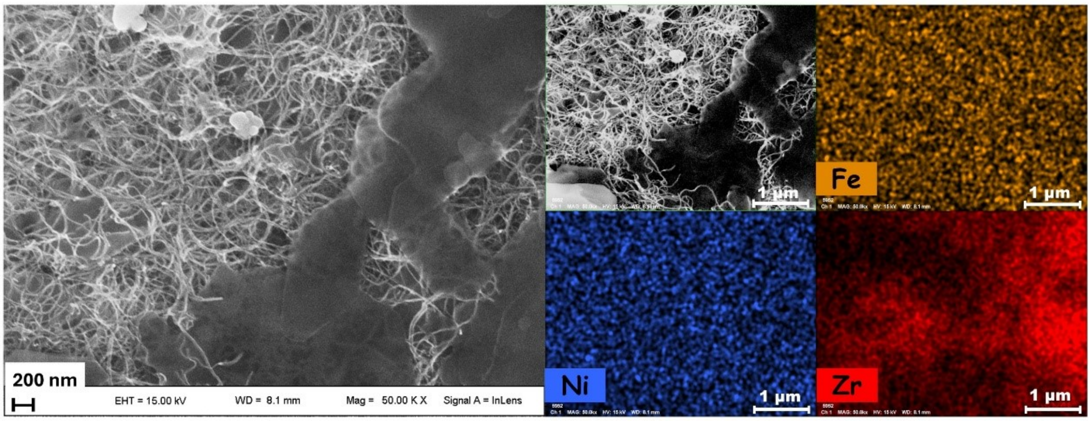

Figure S4. SEM and EDS images of the ink-based NiFeZGABA recorded before (on the top) and after (bottom) the electrochemical reaction.

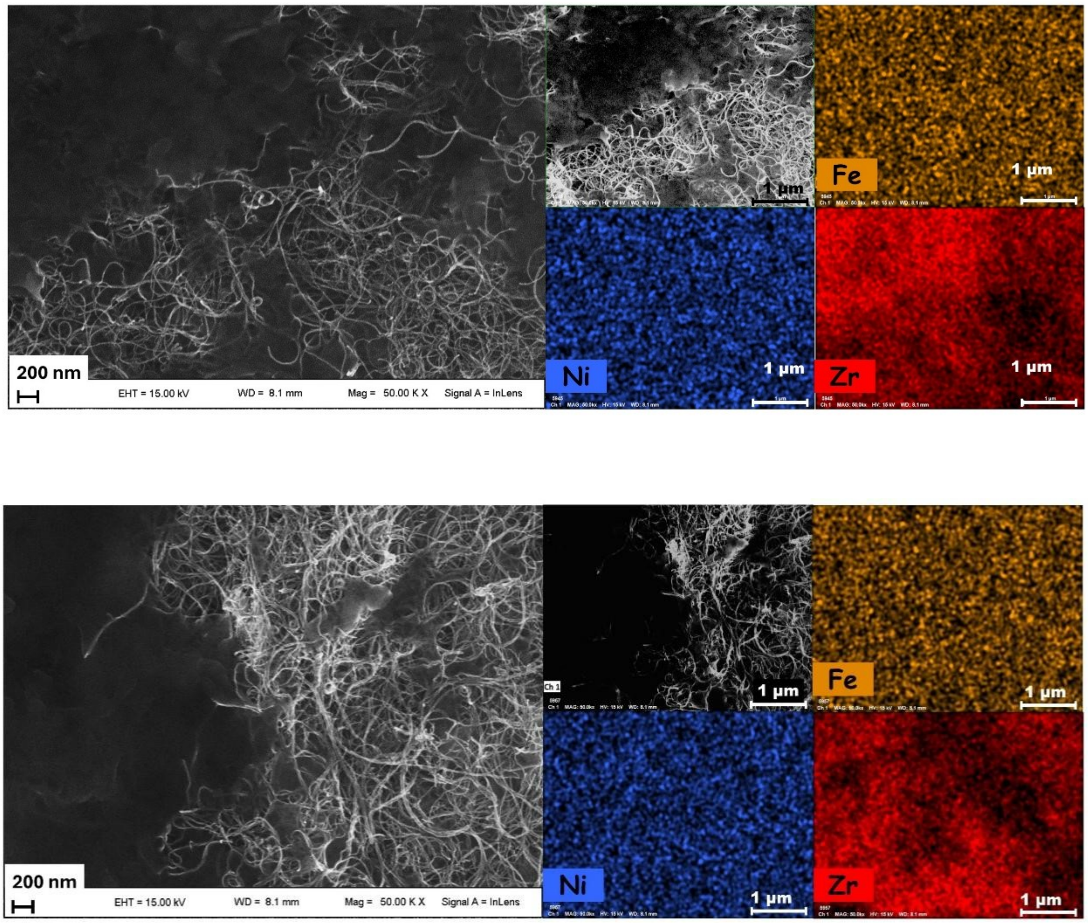

Figure S5. SEM and EDS images of the ink-based NiFeZVAL, recorded before (on the top) and after (bottom) the electrochemical reaction.

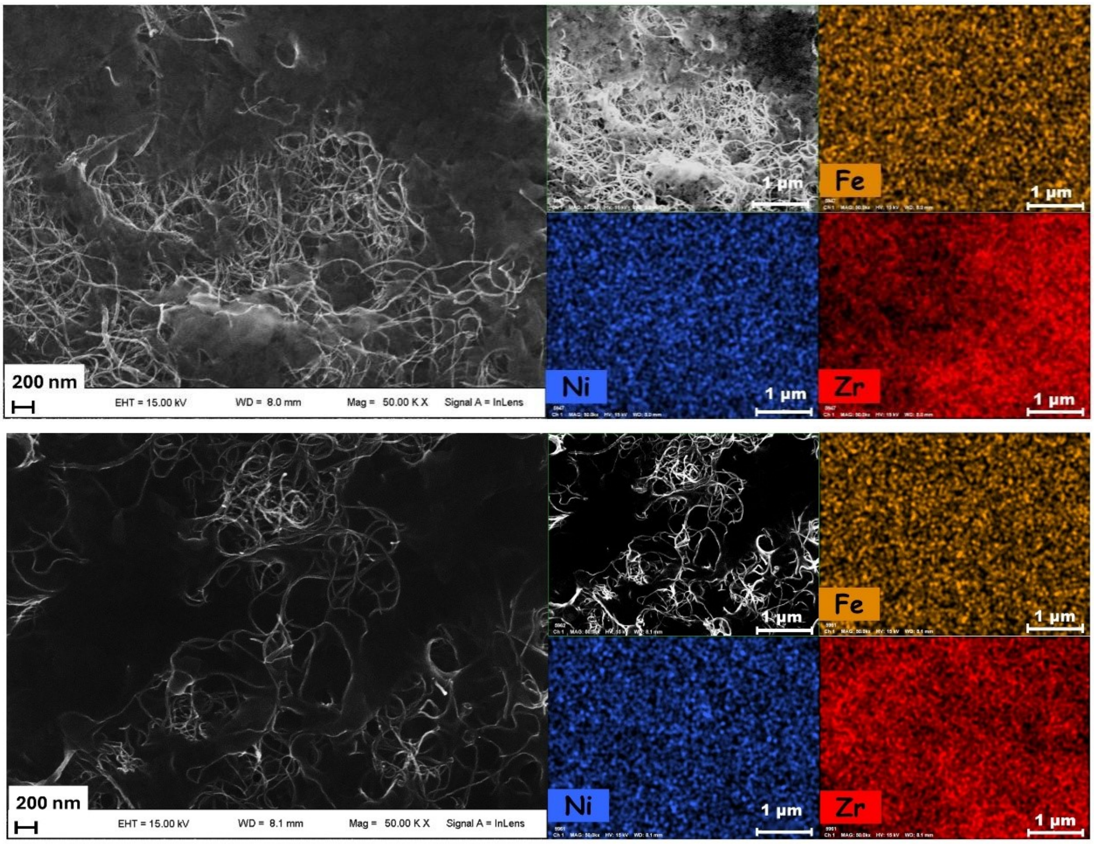

Figure S6. SEM and EDS images of ink-based NiFeZCAP, recorded before (on the top) and after (bottom) the electrochemical reaction.

Table S4. Comparison of the OER performance of representative Ni-Fe-based electrocatalysts in alkaline media. Overpotentials are reported at a geometric current density of 10 mA cm^{-2} (η_{10}).

Catalyst	Electrolyte	η_{10} (mV)	Tafel slope (mV dec^{-1})	Ref.
NiFeZGLY	0.1 M KOH	304	32.9	This work
NiFe intercalated ZrP	0.1 M KOH	340–696	41-220	1
NiFe MOF	0.1 M KOH	240	34	2
Ni/Fe-150/ITO	0.1 M KOH	476	68	3
NiFe LDH/N-rGO	0.1 M KOH	258	63	4
NiFe alloy	0.1 M KOH	275	76	5
NiFe-LDH/CNT	0.1 M KOH	308	35	6
NiFe/C (Ni/Fe=5:5)	0.1 M KOH	320	27	7

NiFe foam etched by HCl	0.1 M KOH	241	44.2	8
rGO/NiFe-LDHNS	0.1 M KOH	254	23	9
IrO_2	0.1 M KOH	336	70.1	8
RuO_2	0.1 M KOH	395	62.9	9
NiFe LDH	1 M KOH	210	39	10
FeOOH NSs@$Ti_3C_2T_x$	1 M KOH	400	95	11
NiCuS@$Ti_3C_2T_x$	1 M KOH	365	58	12
NiFeP@C	1 M KOH	260	76	13
IrO_2	1 M KOH	281	71.7	14

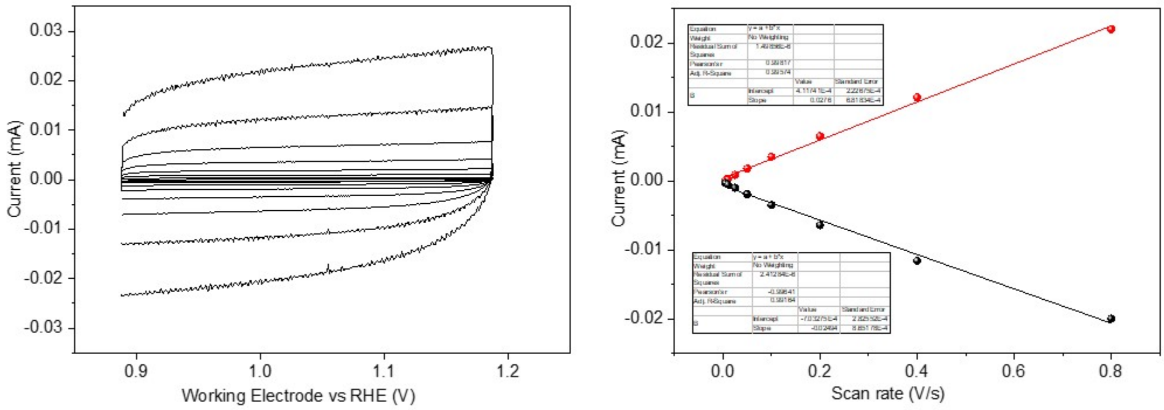

Figure S7. Cyclic voltammograms of $Ni_{0.68}Fe_{0.32}$ZGLY were measured in a non-Faradaic region of the voltammogram at the indicated scan rates. All current is assumed to be due to capacitive charging. (b) The cathodic (red circle) and anodic (black circle) charging currents measured at -0.05 V vs HgO/Hg plotted as a function of scan rate. The determined double-layer capacitance (C_{dl}) of the system is taken as the average of the absolute value of the slope of the linear fits to the data.

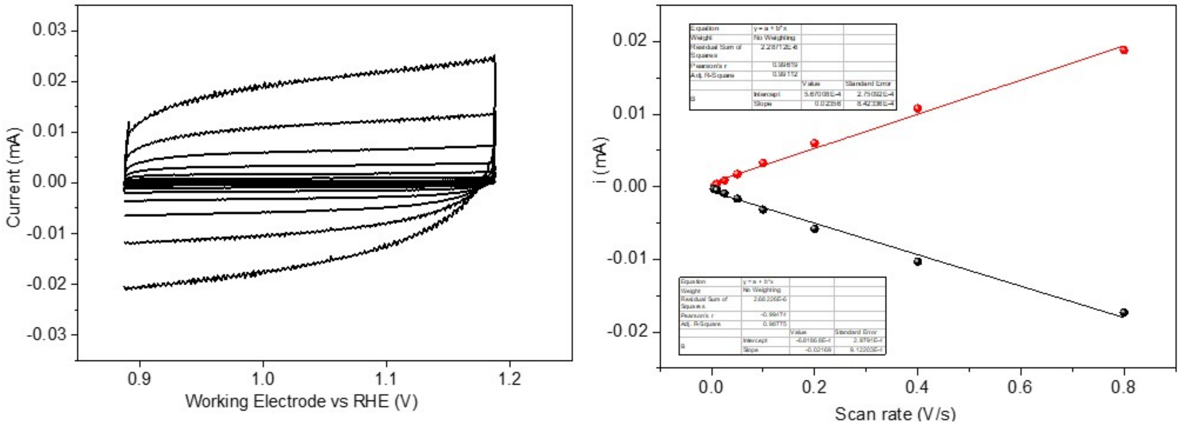

Figure S8. Cyclic voltammograms of NiFeZGABA were measured in a non-Faradaic region of the voltammogram at the indicated scan rates. All current is assumed to be due to capacitive charging. (b) The cathodic (red circle) and anodic (black circle) charging currents measured at -0.05 V vs HgO/Hg plotted as a function of scan rate. The determined C_{dl} of the system is taken as the average of the absolute value of the slope of the linear fits to the data.

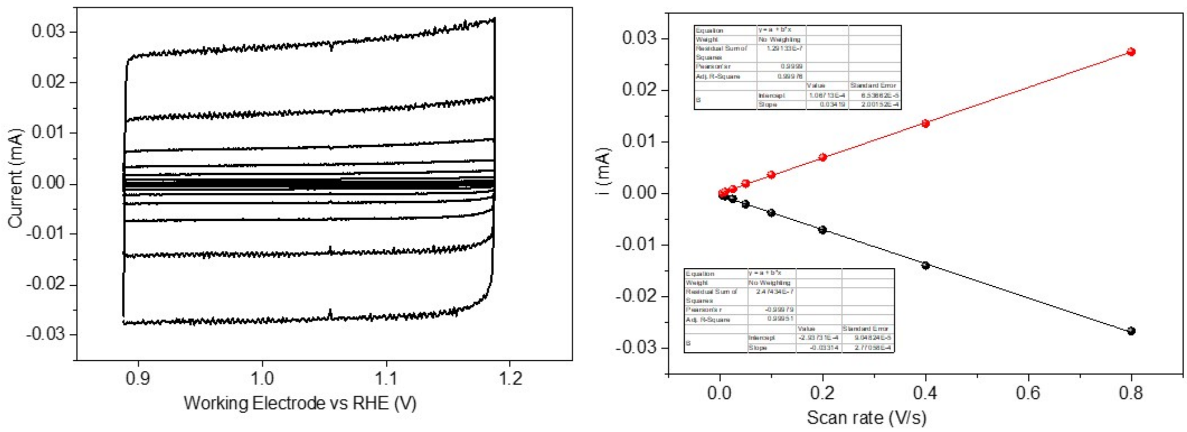

Figure S9. Cyclic voltammograms of NiFeZVAL were measured in a non-Faradaic region of the voltammogram at the indicated scan rates. All current is assumed to be due to capacitive charging. (b) The cathodic (red circle) and anodic (black circle) charging currents measured at -0.05 V vs HgO/Hg plotted as a function of scan rate. The determined C_{dl} of the system is taken as the average of the absolute value of the slope of the linear fits to the data.

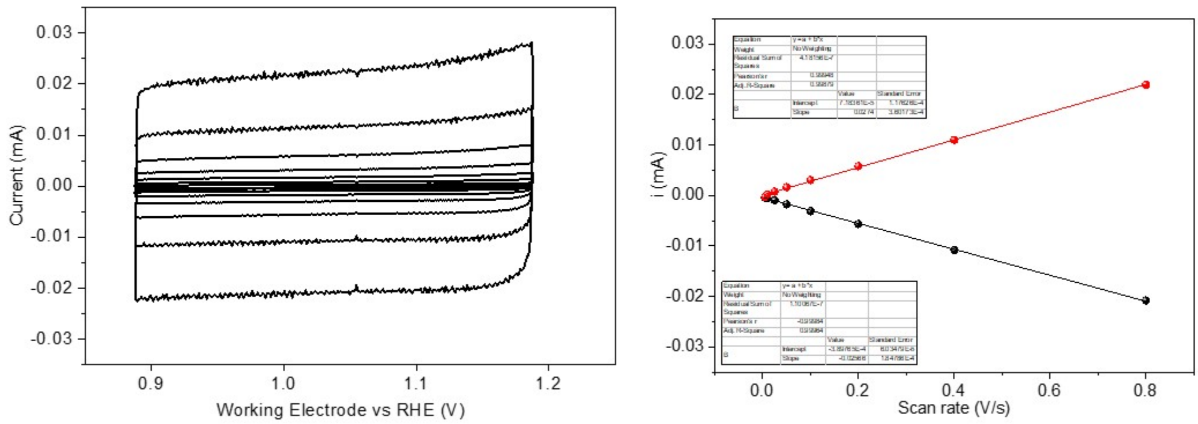

Figure S10. Cyclic voltammograms of NiFeZCAP were measured in a non-Faradaic region of the voltammogram at the indicated scan rates. All current is assumed to be due to capacitive charging. (b) The cathodic (red circle) and anodic (black circle) charging currents measured at -0.05 V vs HgO/Hg plotted as a function of scan rate. The determined C_{dl} of the system is taken as the average of the absolute value of the slope of the linear fits to the data.

Table S5. Comparison of TOF values with representative OER catalysts under alkaline conditions.

Catalyst	**Onset Potential (mV vs. RHE)**	**Tafel Slope (mV dec^{-1})**	**TOF at η=350 mV (s^{-1})**	**Ref.**
$Ni(OH)_2$	254	123.4	0.011	15
IrO_x	248	113.3	0.048	15
NiFe-LDH/CNT	290	35	0.21	16
$Ni_{0.71}Fe_{0.29}(OH)_x$	296	58	0.0146	6
NiFe LDH/C	360	51	0.03	17

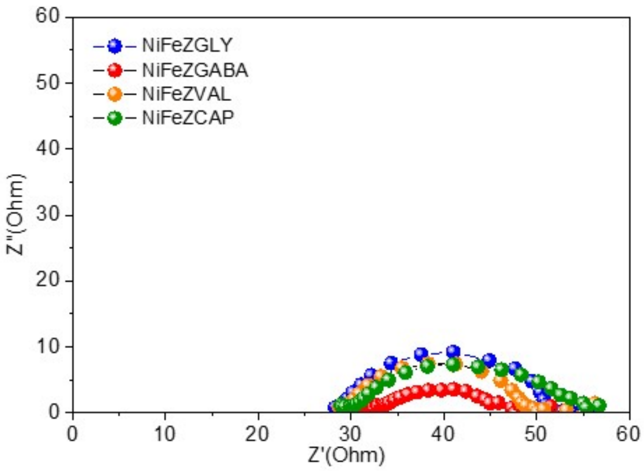

Figure S11. EIS spectra of NiFeZPACs.

Table S6. Binding energy (BE) (in eV) values of Ni, Fe and F elements of inks deposited on FTO. For F the atomic percentage (% at) is also reported.

Ink	**F content (% at)**	**F 1*s* BE**	**Ni 2*p*$_{3/2}$ BE**	**Fe 2*p*$_{3/2}$ BE**	**Other Elements**
$Ni_{0.68}Fe_{0.32}$ZGLY	14.71	688.3	855.4	Not resolved (noisy)	
NiFeZGABA	20.71	688.4	856.1	Not resolved (noisy)	
NiFeZVAL	5.22	688.9	856.1	710.5	
NiFeZCAP	6.01	689.0	856.2	710.6	Sn 3$d_{5/2}$ at 486.7 eV (SnO_2 from FTO)

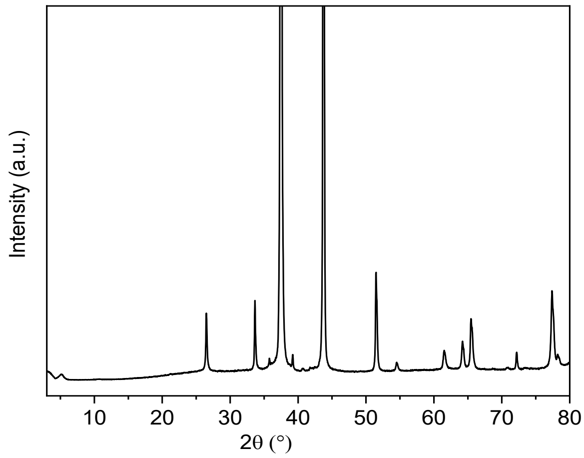

Figure S12. XRD (on the left) and Raman (on the right) analysis on $Ni_{0.68}Fe_{0.32}$ZGLY after chronoamperometric test over 24 hrs under continuous OER operation in alkaline electrolyte. Inset shows representative Raman 2D map (CNTs are shown in red and NiOOH/Fe oxide–oxyhydroxide species formed after the reaction are shown in green).

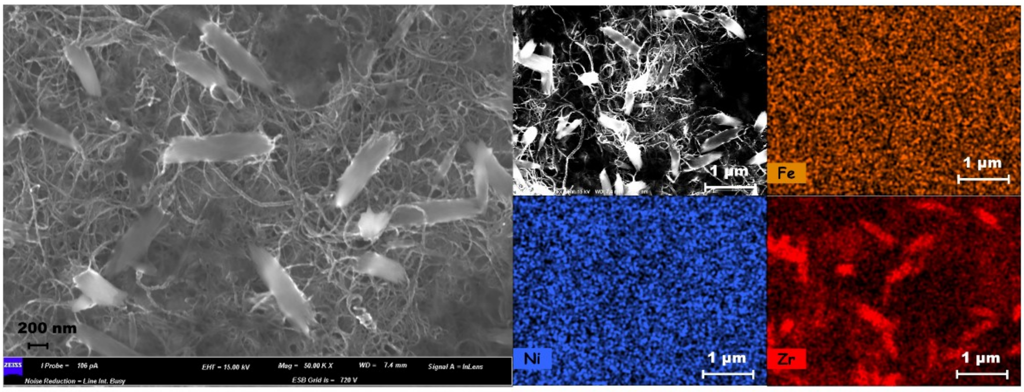

Figure S13. SEM and EDS images of the $Ni_{0.68}Fe_{0.32}$ZGLY recorded after the chronoamperometric test over 24 hrs under continuous OER operation in alkaline electrolyte.

References

1 Sanchez, J., Stevens, M. B., Young, A. R., Gallo, A., Zhao, M., Liu, Y., Ramos-Garcés, M. V., Ben-Naim, M., Colón, J. L., Sinclair, R., King, L. A., Bajdich, M. and Jaramillo, T. F., *Adv. Energy Mater.*, 2021, **11**, 2003545.

2 Duan, J., Chen, S. and Zhao, C., *Nat. Commun.*, 2017, **8**, 15341.

3 Huang, L., Ge, X. and Dong, S., *RSC Adv.*, 2017, **7**, 32819–32825.

4 Cai, Z., Bu, X., Wang, P., Ho, J. C., Yang, J. and Wang, X., *J. Mater. Chem. A*, 2019, **7**, 5069–5089.

5 Mete, S., Sengar, M. S., Dhayal, M., Kumar, V. and Singh, S. K., *J. Mater. Chem. A*, 2024, **12**, 32371–32380.

6 Gong, M., Li, Y., Wang, H., Liang, Y., Wu, J. Z., Zhou, J., Wang, J., Regier, T., Wei, F. and Dai, H., *J. Am. Chem. Soc.*, 2013, **135**, 8452–8455.

7 Sakamaki, A., Yoshida-Hirahara, M., Ogihara, H. and Kurokawa, H., *Langmuir*, 2022, **38**, 5525–5531.

8 Wang, S., Wang, H., Chen, S., Cheung, K. K. K., Wong, H. F., Leung, C. W. and Zapien, J. A., *Int. J. Hydrogen Energy*, 2023, **48**, 17045–17054.

9 Zhan, T., Sun, Y., Wang, Y., Cao, W., Liu, X., Teng, H. and Hou, W., *J. Colloid Interface Sci.*, 2019, **552**, 671–677.

10 Jamesh, M. I., Hu, D., Wang, J., Naz, F., Feng, J., Yu, L., Cai, Z., Colmenares, J. C., Lee, D. J., Chu, P. K. and Hsu, H. Y., *J. Mater. Chem. A*, 2024, **12**, 11771–11820.

11 Zhao, K., Ma, X., Lin, S., Xu, Z. and Li, L., *Chem. Select*, 2020, **5**, 1890–1895.

12 Zou, H., He, B., Kuang, P., Yu, J. and Fan, K., *ACS Appl. Mater. Interfaces*, 2018, **10**, 22311–22319.

13 Kang, Q., Li, M., Shi, J., Lu, Q. and Gao, F., *ACS Appl. Mater. Interfaces*, 2020, **12**, 19447–19456.

14 Yu, F., Zhou, H., Huang, Y., Sun, J., Qin, F., Bao, J., Goddard, W. A. III, Chen, S. and Ren, Z., *Nat. Commun.*, 2018, **9**, 2551.

15 Zhou T., Cao Z., Zhang P., Ma H. Gao Z., Wang H., Lu Y., He J., Zhao Y. Transition metal ions regulated oxygen evolution reaction performance of Ni-based hydroxides hierarchical nanoarrays. Sci. Rep., 2017, **7**, 46154.

16 Gao Y. Q., Liu X.Y., Yang G. W., Amorphous mixed-metal hydroxide nanostructures for advanced water oxidation catalysts, Nanoscale, 2016, **8**, 5015–5023.

17 Dionigi F., Strasser P. Adv. Energy Mater. 2016, **6**, 1600621.